Appl Phys A (2009) 97: 751–757
DOI 10.1007/s00339-009-5350-8

Applied Physics A
Materials Science & Processing

Fabrication of microlens arrays in photosensitive glass by femtosecond laser direct writing

C.H. Lin · L. Jiang · Y.H. Chai · H. Xiao · S.J. Chen · H.L. Tsai

Received: 5 May 2009 / Accepted: 13 July 2009 / Published online: 29 July 2009
© Springer-Verlag 2009

Abstract This article reports the fabrication of high-fill-factor plano-convex cylindrical and spherical microlens arrays horizontally and vertically embedded in a photosensitive Foturan glass chip by femtosecond (fs) laser micromachining. The microlens arrays were fabricated by modifying the microstructure of Foturan glass using fs laser direct writing followed by thermal treatment, wet etching, and additional annealing. The focusing ability and image quality of the microlens arrays were examined, showing that the lens arrays not only can focus light well but also provide an imaging capability that holds great potential for lab-on-a-chip applications.

PACS 42.62.-b · 81.05.Kf · 82.50.Pt

C.H. Lin · S.J. Chen
Department of Engineering Science, National Cheng Kung University, Tainan 70101, Taiwan

C.H. Lin · H.L. Tsai (✉)
Department of Mechanical & Aerospace Engineering, Missouri University of Science and Technology, Rolla, MO 65409, USA
e-mail: tsai@mst.edu
Fax: +1-573-3414607

L. Jiang
Department of Mechanical and Automation Engineering, Beijing Institute of Technology, Beijing 100081, China

Y.H. Chai
Department of Electrical Engineering, Technology and Science Institute of Northern Taiwan, Taipei 112, Taiwan

H. Xiao
Department of Electrical & Computer Engineering, Missouri University of Science and Technology, Rolla, MO 65409, USA

1 Introduction

Recently, the development of 'lab-on-a-chip' or micro-total analysis systems (μ-TAS) has attracted a lot of attention in analytical chemistry and biomedical applications because of the advantages of low reagent consumption, fast analysis, compactness of the system, ease of operation, etc. [1]. The latest advancement and trend of μ-TAS have been reviewed from the standpoints ranging from the materials being used for microchips, the manufacturing technology, and the analytical operations and applications [2]. A μ-TAS can be fabricated by means of integrating functional microcomponents, such as microfluidic devices, micromechanics, optical waveguides, and optics, into a single chip to enable on-chip measurements. Although the fabrication of individual optical or mechanical components has been accomplished [3, 4], the additional assembly and alignment of microcomponents into a single chip is still a challenge. In many photonic sensing applications, a microlens is the critical component due to its functions of focusing light into a microfluidic channel, collecting more fluorescence signals to enhance the signal-to-noise ratio [5], or providing imaging capability. Recently, horizontal microlens arrays integrated in a microchip to perform multichannel or microarray analysis have been demonstrated in sensing applications [6, 7]. In many lab-on-a-chip applications, 3D microlenses vertically embedded in transparent material are desirable [5].

Microlens arrays have been widely used in different applications such as beam shaping and steering [8], display and imaging [9], microfluidic sensing [5–7], waveguide coupling [10], and wavefront detection [11]. Many techniques have been developed to fabricate microlens arrays, including droplet injection [12], photoresist reflow [13], gray-tone photolithography [14], and mask-free direct writing

(focused ion-beam machining [15] and direct laser writing [16]). Compared to the direct writing method, the mask-based photolithography technique has a relatively lower cost and higher production rate, but its significant drawbacks include the difficulty of achieving arbitrary surface curvatures and positioning the lens in a vertical direction. In the direct writing technique, the focused ion-beam method provides flexibility to machine an arbitrary surface profile, but it has to be performed in a vacuum chamber and cannot achieve 3D embedded structures inside the specimen. Based on the femtosecond (fs) laser direct writing technique, the multiphoton polymerization technique provides a bottom-up approach for the fabrication of 3D micro/nanoscale structures with an arbitrary shape [17]. Generally, this method is suitable for fabricating microchips with complicated functional designs. However, it is difficult, if not impossible, to fabricate microchips containing a few hollow microstructures, such as internal microchannels and microlenses, using the multiphoton polymerization technique.

Materials for microchips should contain properties such as optical transparency in the visible-light region as well as resistance to corrosion. Foturan glass with photosensitive characteristics has been used for microstructure fabrication [18, 19] and the detailed procedure for processing Foturan glass can be found elsewhere [20]. Foturan glass machined by a fs laser can achieve the one-step fabrication (i.e. without further assembly or alignment) of microstructures with several components in a single chip. It greatly simplifies the chip fabrication process and it is easier to achieve complicated designs. In this work, we employed a fs laser direct writing technique to fabricate horizontal and vertical microlens arrays embedded in photosensitive Foturan glass. The arrays provide very good focusing properties as well as imaging capabilities, which reveal great potential for the lab-on-a-chip or μ-TAS applications.

2 Experimental

The fs laser system used in the experiment is a regeneratively amplified Ti:sapphire laser (Legend-F, Coherent) whose repetition rate, center wavelength, and pulse duration are 1 kHz, 800 nm, and 120 fs, respectively. The maximum output power of the fs laser is 1 W, which corresponds to a pulse energy of 1 mJ. The laser beam was attenuated and coupled into a microscope objective lens (Olympus) and then focused into the glass sample. The Foturan glass (Mikroglas Chemtech) sample was mounted on a computer-controlled five-axis motion stage (Aerotech) with a resolution of 1 μm. The whole process was monitored via an in-line imaging system integrated into the fs laser micromachining system.

Several laser writing programs were implemented to fabricate different microlens arrays. The schematic diagram of

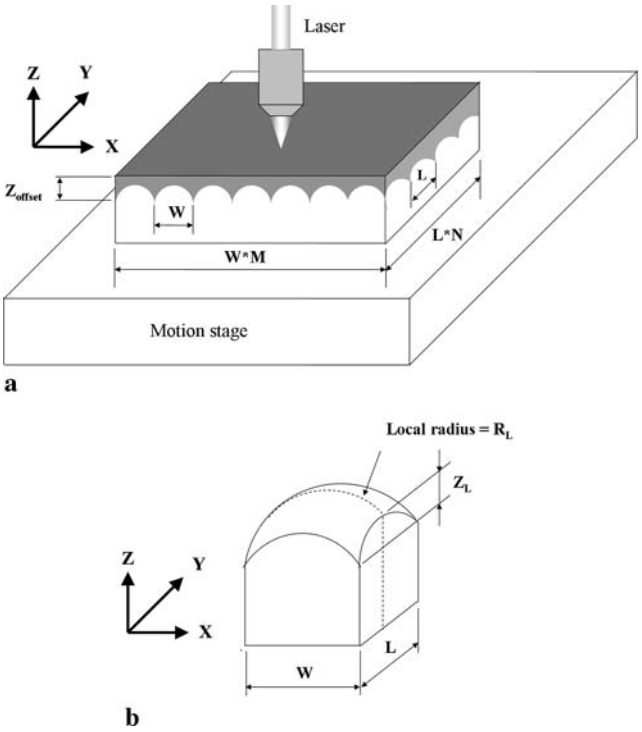

Fig. 1 Schematic diagram of the laser scanning process. **a** Overview; **b** one lens

the laser scanning process is illustrated in Fig. 1a. In the horizontal lens fabrication, the process consists of periodic curve scanning in a sliced X–Z plane along the X direction and the layer-by-layer processing along the Z direction. To facilitate the following discussion, as shown in Fig. 1b for a single lens, we denote R as the radius of the surface curvature, L as the length (Y direction), and W as the width (X direction). M is the number of lenses in each row (X direction) and N is the number of lenses in each column (Y direction). Hence, an $M \times N$ lens array means that in the X–Y plane there are M lenses in the X direction and N lenses in the Y direction. To fabricate a spherical microlens array, the computer program consists of the following five steps: (1) move the glass sample toward the objective lens by a desired offset distance Z_{offset} which is calculated from the given parameters R, L, and W. Then, set the position as the origin ($X = 0$, $Y = 0$, $Z = 0$); (2) calculate the local curvature radius R_{L} and local offset Z_{L} and then move the sample to the position with distance Z_{L} along the positive Z direction. As shown in Fig. 1b, R_{L} is the local 2D curvature radius in each sliced X–Z plane and Z_{L} is the offset distance from the origin ($Z = 0$) to the starting point in each sliced X–Z plane; (3) scan horizontally a number M of vertical arcs one-by-one in the X–Z plane along the X axis with radius R_{L} and chord W; (4) shift the sample by a predetermined distance, D_{slice}, in the Y direction and repeat the aforementioned steps (2) and (3) until the length of the scanned area along the Y axis has progressed to $N \times L$ μm; (5) shift in the Z direc-

tion by a predetermined distance, D_{layer}, and scan another layer. The entire process was repeated until the calculated numbers of layers were completed.

For the cylindrical microlens array, the aforementioned process was simplified by setting the radius R_L equal to R and Z_L to 0. Thus, the cylindrical microlens array along the Y direction can be fabricated by changing the parameters in the same program. In this design, an array consisting of lens elements with a close-contact rectangular boundary was fabricated. For vertical microlens arrays, the sliced plane was changed to the X–Y plane and the layer by layer direction was changed to the Y direction. A distance compensation function, which was calculated using the parameters of the refractive index of Foturan glass and the numerical aperture (NA) of the objective lens, was also added in the program to compensate for spherical aberrations caused by the refractive-index mismatch between air and glass at their interface [21]. Furthermore, a 0.2-mm slit was put before the objective lens to shape the intensity distribution at the focal plane [22–24]. This will decrease possible distortion of the shape of the vertical microlens array.

In the case of the horizontal microlens array, the applied laser pulse energy before the objective lens was measured to be 160 nJ, which is lower than the pulse energy used previously [3]. The lower pulse energy leads to the exposing of the Foturan glass over a smaller effective area, which improves the accuracy for a 3D curved surface. In the case of the vertical microlens array, the applied laser pulse energy before the slit was 14 μJ because most energy is blocked by the slit which is placed before the objective lens. In all experiments, a ×20 objective lens with NA of 0.46 was used and the scanning speed was set as 20 mm/min. For all experiments, D_{slice} and D_{layer} were set as 1 μm and 8 μm, respectively. D_{slice} directly affects the surface roughness, so it should be as small as possible.

After the laser scanning process, the sample was thermally treated inside a programmable furnace (Fischer Scientific) to develop the modified region inside the sample. The temperature was first ramped up to 500°C at 5°C/min and held at this temperature for 1 h. It was then raised to 600°C at 3°C/min and held for another hour. After this thermal treatment, the furnace power was turned off and the sample was kept inside the furnace until the temperature was gradually cooled to room temperature. At this stage, the crystalline phase of the Foturan glass developed at the laser-exposed region becomes a brown color and the nonmodified amorphous phase is still clear, allowing visual confirmation of the 3D structure. The cooled sample was then soaked in a solution of 10% hydrofluoric (HF) acid in an ultrasonic bath for 15 min to remove all modified volumes and then rinsed. Lastly, the etched sample was baked again at 560°C for 5 h for further smoothing the surface of the microlens array. The focus quality and image performance of the microlens array were examined.

3 Results and discussion

3.1 Cylindrical microlens arrays

After the fs laser scanning, heat treatment, wet etching, and additional annealing, three plano-convex cylindrical microlens arrays embedded in the photosensitive Foturan glass were fabricated. These include a 10 × 1 horizontal array (i.e. X–Y plane, Fig. 1) with the lens axis along the Y direction (case C1), a 5 × 1 vertical array (i.e. X–Z plane) with the lens axis along the Z direction (case C2), and a 1 × 2 vertical array (i.e. X–Z plane) with the lens axis along the X direction (case C3). Both the radius of the surface curvature and the chord for each lens are 150 μm. Figure 2a, b, and c are the scanning electron microscope (SEM) images of cases C1, C2, and C3, respectively. Figure 2d and e show the surface morphologies for case C1 before and after the annealing process at 560°C for 5 h. It is seen that the annealing process is essential in order to achieve a 'smooth' surface. Previous investigations showed an average roughness of about 80 nm before annealing and about 0.8 nm after a second annealing could be achieved for a planar structure with a scanning area of 20 μm × 20 μm [25]. In this study it is estimated that the averaged surface roughnesses before and after annealing are, respectively, about 100 nm and 2 nm.

Next, we examine the focusing ability of the cylindrical microlens arrays. An expanded He–Ne laser whose output power and beam diameter are, respectively, 1 mW and 2.5 mm was used as a narrowband light source to minimize the chromatic aberration. The laser intensity distribution at the focal plane of the lens array was observed and recorded by a monochrome CCD camera. Figure 3a is the image of the narrow line array focused by the case C1 lens array using a ×4 objective lens. This low-magnification image reveals an array of focused lines corresponding to the array of cylindrical microlenses. The collimating laser beam is focused into periodic narrow lines with a pitch of 150 μm, which is consistent with the designed dimension. An enlarged image of a focused line was also taken using a ×20 objective lens, Fig. 3b, to determine the focusing quality. The cross-sectional profiles of a focused line from the enlarged image are shown in Fig. 3c for case C1 (solid line), case C2 ('o' sign), and case C3 ('*' sign). The full width at half maximum (FWHM) of focused lines for the cases C1 through C3 are, respectively, 5.0 μm, 4.9 μm, and 6.3 μm. It is seen that, for all cases, a much better focus than previously obtained [3] is achieved.

3.2 Spherical microlens arrays

A 10 × 10 horizontal array (i.e. X–Y plane) of plano-convex spherical microlenses (case S1) and a 5 × 1 vertical array (i.e. X–Z plane; case S2) were fabricated. A single lens is

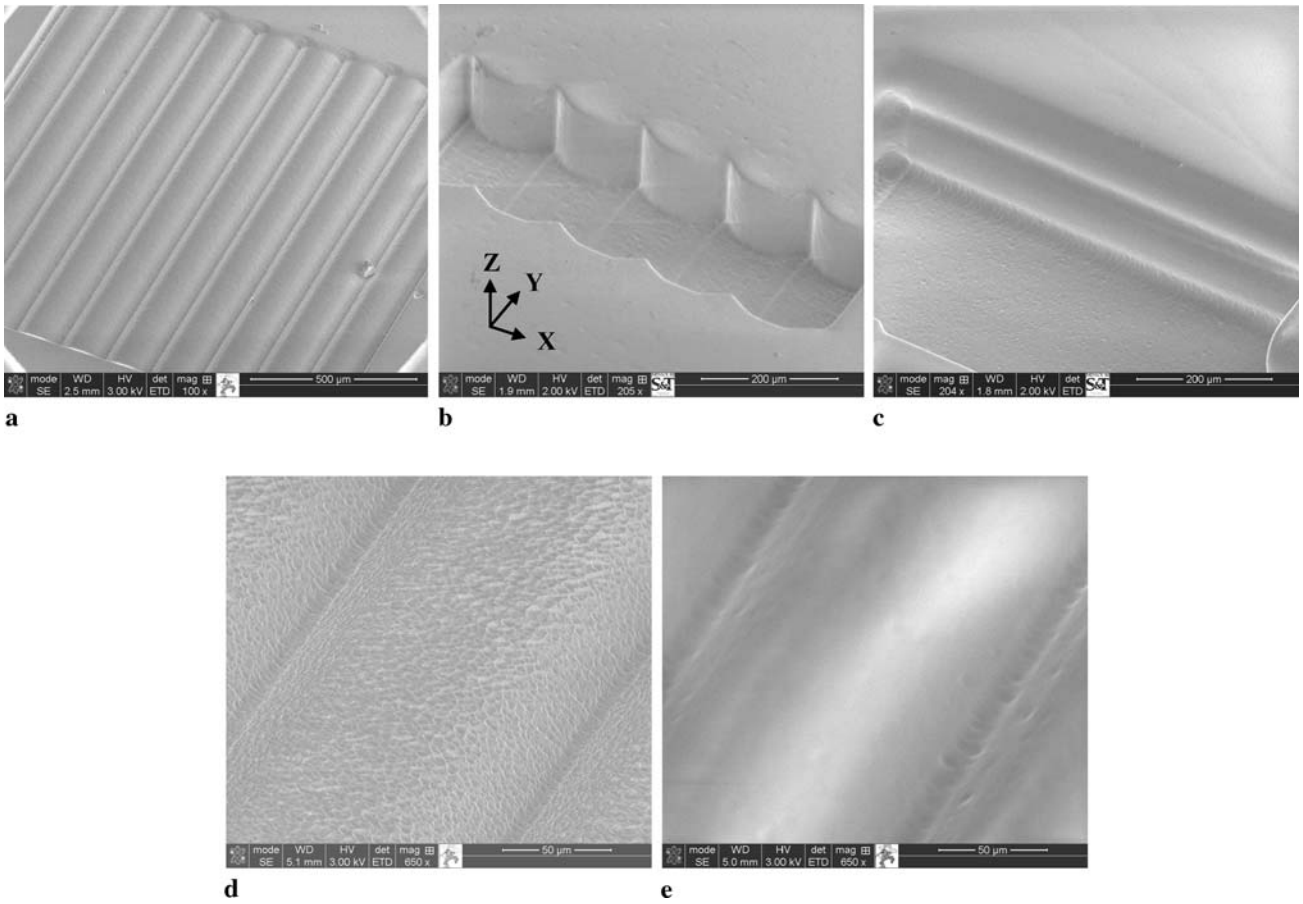

Fig. 2 SEM images of the plano-convex cylindrical microlens array. **a** A 10 × 1 horizontal microlens array; **b** a 5 × 1 vertical array with horizontal focusing orientation; **c** a 1 × 2 vertical array with vertical focusing orientation; **d** an enlarged image of the microlens before the annealing process; **e** an enlarged image of the microlens after the annealing process

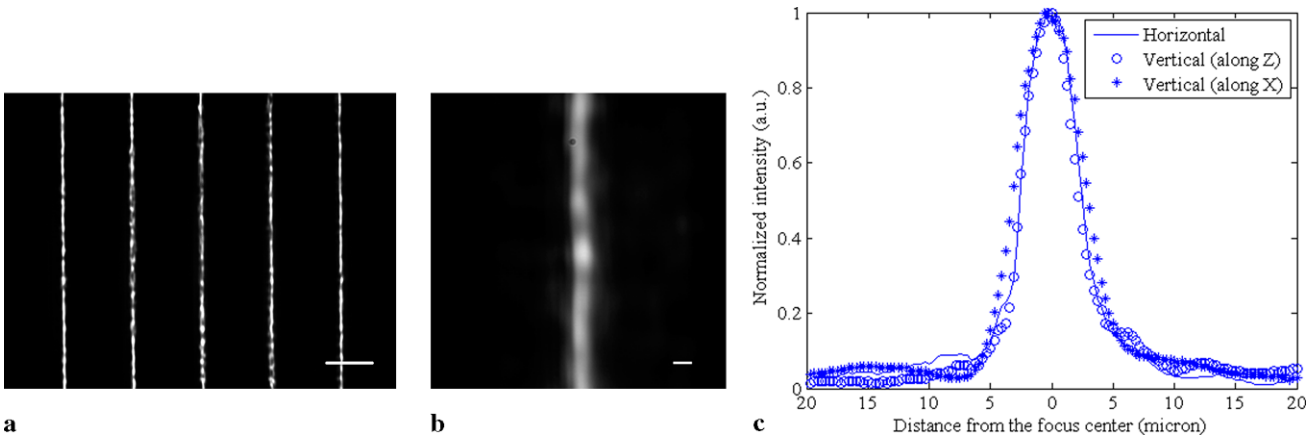

Fig. 3 Focal plane images of the plano-convex cylindrical microlens array. **a** The image of the focusing line array using a ×4 objective lens (the scale bar is 100 μm); **b** enlarged image of the focused line shape with a ×20 objective lens (the scale bar is 10 μm); **c** the cross-sectional profile

150-μm square and has a curvature radius of 150 μm. The SEM images of cases S1 and S2 are shown in Fig. 4. The array of focused spots and an enlarged single focal spot are shown in Fig. 5a and b, respectively. Unlike the regular circular shape of a lens with a circular aperture, the shape of the focused spot is close to rectangular, which is consistent with Fourier's transformation of the rectangular aperture of each spherical lens [26]. The FWHM of the cross-sectional

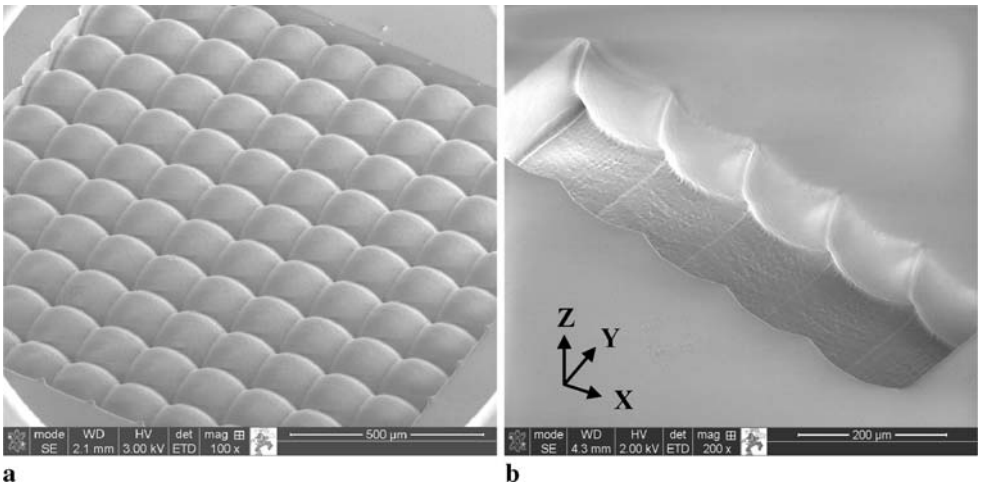

Fig. 4 SEM images of the plano-convex spherical microlens arrays. **a** A 10 × 10 horizontal array; **b** a 1 × 5 vertical array

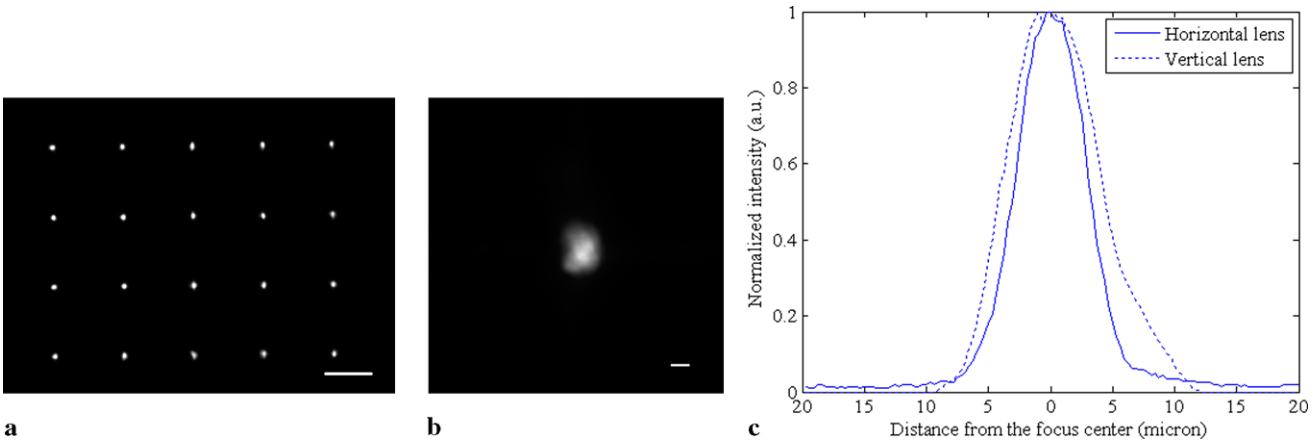

Fig. 5 Focal plane images of the plano-convex spherical microlens array. **a** The image of the focusing line array using a ×4 objective lens (the scale bar is 100 μm); **b** enlarged image of the focused line shape with a ×20 objective lens (the scale bar is 10 μm); **c** the cross-sectional profile

profile for the spot in case S1 is 6.5 μm and is 8.7 μm for case S2, Fig. 5c. In case S1, the focused spot size agrees with the measured focused line width for the cylindrical lens array as shown in Fig. 3c. In case S2, the spot size is 34% larger than that in case S1 because of the shape distortion during the vertical lens fabrication.

As the laser beam has been expanded to fill the entire lens array, the beam size is the same as the entrance aperture, which is 150 μm. For the He–Ne laser with 632.8-nm wavelength, the spherical lens with 300-μm focal length, and the Foturan glass with 1.5 refractive index, the calculated theoretical focal spot size (diameter of the Airy disk) is 3.183 μm. However, the measured FWHM of the focal spot size is 6–8 μm and the width of the 10% intensity is around 12 μm, which is about four times the theoretical value. This can be attributed to (1) the surface roughness of the lens; (2) the bulk deformation of the lens; and (3) the compositional uniformity of the Foturan glass. In the final annealing process, the annealing temperature must be higher than the transition temperature of the glass to form a thin melted layer on the glass surface. In general, the bulk glass starts to become soft when the treating temperature is slightly higher than the transition temperature. The formation of a thin melting layer on the surface is the major mechanism to smooth the surface. The melted layer should be thin to match the roughness of the machined surface before annealing and to allow the surface tension to act and smooth the surface. A thicker melted layer may cause a smoother surface but it also may cause thermal distortion. The annealing process was optimized using several samples under different annealing parameters. The focusing quality of all annealed samples was examined to decide the optimized annealing condition. The optimized annealing temperature was found to be 560°C, which is close to the average of the glass-transition temperature and the melting temperature. In addition to the basic focusing ability, the imaging performance of the spherical lens array was also examined.

A micro 'MST' target was machined on a microscope slide by the same fs micromachining system. The dimensions of each character are 20 μm × 20 μm and the gap be-

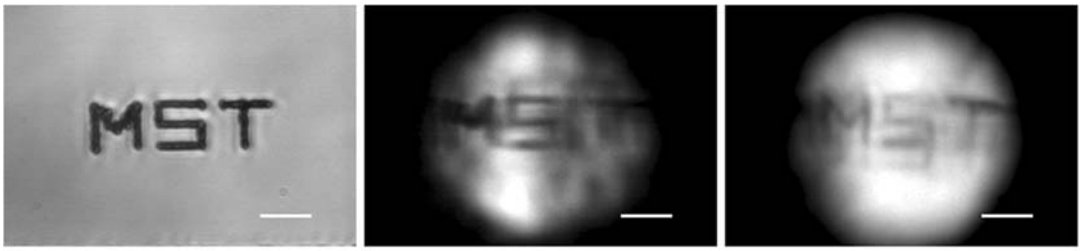

Fig. 6 Imaging performance of the spherical microlens array. **a** A 'MST' pattern fabricated by a femtosecond laser; **b** an image of the 'MST' pattern projected by an element of the horizontal microlens array; **c** an image of the 'MST' pattern projected by an element of the vertical microlens array. The scale bar is 20 μm

tween adjacent characters is 10 μm. The bright-field image of the target is shown in Fig. 6a. The target was used as an objective for the imaging testing, and it was placed in front of the lens array at a distance of 600 μm, which corresponds to a distance of $2f$ for a lens element with a curvature radius of 150 μm. To prevent possible image overlapping between lens elements, no magnification was used. A $\times 10$ objective lens was used to take the enlarged image of the 'MST' target formed by the spherical lens unit of the entire lens array for both cases S1 and S2. As shown in Fig. 6b and c, the size of the 'MST' image formed by the microlens is the same as the size of the original target which is defined by our testing design. In this setup, the image was formed inside the glass chip due to the chip thickness being greater than $2f$. This situation can degrade the image quality since the back surface of the glass may have been deformed during the annealing process.

3.3 Potential applications

In this work, the cylindrical microlens array with a vertical focusing orientation (case C3) and the vertical spherical microlens array (case S2) are true 3D microstructures and they cannot be fabricated by a lithography-based technique due to the change of cross-sectional shapes in the Z direction. Although the distortion of the vertical spherical microlens is significantly larger than the horizontal one during the fabrication process, several compensations were performed to minimize the possible distortion. The focusing ability of the well-fabricated microlens arrays still focuses light into tiny spots in the scale of 6–8 μm (FWHM). From the results, the microlens arrays with horizontal or vertical orientations reveal high focusing quality and image performance. The high-fill-factor structure provides highly efficient performance in photonics applications. This embedded 3D lens array can be easily integrated into a lab-on-a-chip for either focusing an optical beam into a microfluidic channel for fluorescence detection or even creating an image of a dynamic process in a microfluidic chamber. The vertical embedded microlens arrays open an opportunity to realize microchips with a 3D-distributed dense microfluidic channel for complicated functional chip designs.

4 Conclusions

In conclusion, the fabrication of horizontal and vertical microlens arrays in photosensitive Foturan glass using a fs laser micromachining system operated at near-infrared wavelengths has been demonstrated. The fs induced multiphoton absorption inside the Foturan glass was employed to develop a 3D top-down fabrication technique for microstructures with arbitrary shapes and precise dimensions. The focusing performance and imaging quality of the lens arrays were examined. The microlens arrays were proven to be capable of tightly focusing light and also providing imaging capability, which demonstrate high potential for the integration with other microcomponents in the lab-on-a-chip or μ-TAS applications.

References

1. P. Yager, T. Edwards, E. Fu, K. Helton, K. Nelson, M.R. Tam, B.H. Weigl, Nature **442**, 412 (2006)
2. P.S. Dittrich, K. Tachikawa, A. Manz, Anal. Chem. **78**, 3887 (2006)
3. Y. Cheng, H.L. Tsai, K. Sugioka, K. Midorikawa, Appl. Phys. A **85**, 11 (2006)
4. Y. Bellouard, A.A. Said, P. Bado, Opt. Express **13**, 6335 (2005)
5. K.W. Ro, K. Lim, B.C. Shim, J.H. Hahn, Anal. Chem. **77**, 5160 (2005)
6. K.S. Hong, J. Wang, A. Aharonov, D. Chandra, J. Aizenberg, S. Yang, J. Micromech. Microeng. **16**, 1660 (2006)
7. S. Park, Y. Jeong, J. Kim, K. Choi, H.C. Kim, D.S. Chung, K. Chun, Jpn. J. Appl. Phys. **45**, 5614 (2006)
8. A. Akatay, H. Urey, Opt. Express **15**, 4523 (2007)
9. C.P.B. Siu, H. Zeng, M. Chiao, Opt. Express **15**, 11154 (2007)
10. M. He, X.C. Yuan, N.Q. Ngo, J. Bu, S.H. Tao, J. Opt. A **6**, 94 (2004)
11. G.Y. Yoon, T. Jitsuno, M. Nakatsuka, S. Nakai, Appl. Opt. **35**, 188 (1996)
12. V. Bardinal, E. Daran, T. Leichle, C. Vergnenegre, C. Levallois, T. Camps, V. Conedera, J.B. Doucet, F. Carcenac, H. Ottevaere, H. Thienpont, Opt. Express **15**, 6900 (2007)

13. P. Nussbaum, R. Volkel, H.P. Herzig, M. Eisner, S. Haselbeck, Pure Appl. Opt. **6**, 617 (1997)
14. J. Yao, Z. Cui, F. Gao, Y. Zhang, Y. Guo, C. Du, H. Zeng, C. Qiu, Microelectron. Eng. **57–58**, 729 (2001)
15. Y.Q. Fu, N. Kok, A. Bryan, Microelectron. Eng. **54**, 211 (2000)
16. A.Y. Smuk, N.M. Lawandy, J. Appl. Phys. **87**, 4026 (2000)
17. S. Kawata, H.B. Sun, T. Tanaka, K. Takada, Nature **412**, 697 (2001)
18. M. Masuda, K. Sugioka, Y. Cheng, T. Hongo, K. Shihiyama, H. Takai, I. Miyamoto, K. Midorikawa, Appl. Phys. A **78**, 1029 (2004)
19. Y. Cheng, K. Sugioka, K. Midorikawa, Opt. Express **13**, 7225 (2005)
20. T. Hongo, K. Sugioka, H. Niino, Y. Cheng, M. Masuda, I. Miyamoto, H. Takai, K. Midorikawa, J. Appl. Phys. **97**, 063517 (2005)
21. F.L. Pedrotti, L. Pedrotti, L.M. Pedrotti, L.S. Pedrotti, *Introduction to Optics* (Benjamin Cummings, New Jersey, 2006)
22. Y. Cheng, K. Sugioka, K. Midorikawa, M. Masuda, K. Toyoda, M. Kawachi, K. Shihoyama, Opt. Lett. **28**, 55 (2003)
23. G. Cerullo, R. Osellame, S. Taccheo, M. Marangoni, D. Polli, R. Ramponi, P. Laporta, S. De Silvestri, Opt. Lett. **27**, 1938 (2002)
24. K.J. Moh, Y.Y. Tan, X.C. Yuan, D.K.Y. Low, Z.L. Li, Opt. Express **13**, 7288 (2005)
25. Y. Cheng, K. Sugioka, K. Midorikawa, M. Masuda, K. Toyoda, M. Kawachi, K. Shihoyama, Opt. Lett. **28**, 1144 (2003)
26. J.W. Goodman, *Introduction to Fourier Optics*. McGraw-Hill Ser. Electron. Comput. Eng. (McGraw-Hill, New York, 1996)